# Experimental study of how far blood spatter stains on fabrics can be found from the blood source, and relevance to crime scene reconstruction

Richard Faflak[1] (r.faflak@gmail.com), Daniel Attinger[1,2] (struoattinger@gmail.com),
[1] Department of Mechanical Engineering
Iowa State University, IA, USA
[2]Struo LLC
Ames, IA, USA

## Abstract

For investigative purposes, the bloodstain pattern analyst might have to estimate if a given stain on fabric could have originated from a specific location. A wide range of values of the maximum distance that a blood drop can travel have been reported based on experiments, ranging from less than 1 m to more than 10 m. It is also known that stains on porous materials such as fabrics are more difficult to interpret than stains on non-absorbing surfaces, because of wicking. Here we perform several fluid dynamic spatter experiments and formulate a fluid dynamics model to describe the trajectories of the blood drops. The experiments are performed with swine blood, the properties of which are well understood. The main parameters screened are the drop size, initial velocity, the launch angle, and the orientation of the fabric. A large number of blood drops are produced by impact or gunshot events. The resulting stains on knitted white T-shirt fabric are digitally measured. Their position relative to the source and size is reported. Trajectories are simulated accounting for the influence of gravity and drag forces. A simple relation between drop size and stain size is established based on extensive experiments on a specific fabric. Results of the trajectory simulations are then searched and mined for parameters directly measurable on a crime scene, such as the stain size on fabric and the relative location of the fabric with respect to the blood source. The experimental results are compared and found in agreement with the numerical predictions. The results are presented in one chart relevant to crime scene reconstruction. The chart is easy to use, and only requires minimum knowledge of fluid dynamics.

## Declarations

**Funding:** US National Institute of Justice – Office of Justice Programs (award 2017DN-BX-017)

**Conflicts of interest/Competing interests:** None

**Availability of data and material:** Data is described in manuscript

**Code availability:** None

**Acknowledgements:** The authors acknowledge Dr. James Michael of Iowa State University for providing feedback on this manuscript.

**Keywords**: BPA; bloodstain; fabrics; trajectory; maximum distance; spatter

# 1. INTRODUCTION

Following criticisms in a 2009 report on the scientific basis of forensics disciplines by the US National Research Council (NRC 2009) , governmental agencies such as the US National Institute of Justice have encouraged physics-based research in forensics. Over the last decade, several peer-reviewed studies (Buck and Kneubuehl 2012, Adam 2013, Attinger, Moore et al. 2013, Camana 2013, Kabaliuk, Jermy et al. 2014, Cho, Springer et al. 2015, Laan, de Bruin et al. 2015, Comiskey, Yarin et al. 2016, Kim, Ma et al. 2016, Kolbasov, Comiskey et al. 2016, Comiskey, Yarin et al. 2017, Comiskey, Yarin et al. 2017, Kröll, Kettner et al. 2017, Siu, Pender et al. 2017, Arthur, Hoogenboom et al. 2018, Comiskey, Yarin et al. 2018, Feng, Michielsen et al. 2018, Shiri, Martin et al. 2018, Attinger 2019, Comiskey and Yarin 2019) have addressed specific challenges in the forensic discipline of bloodstain pattern analysis (BPA). These studies focused on providing quantitative, physics-based understanding of the properties of blood, the physical formation of blood drops, the flight of drops, and their impact and drying on a variety of target materials. The need for physics-based research can be justified by the multiple and natural connections between fluid dynamics and bloodstain pattern analysis (Attinger, Moore et al. 2013) . That latter reference describes the fluid dynamics concepts relevant to BPA, through theory and examples. Some of these recent studies are briefly summarized hereafter, and their relevance to BPA is highlighted.

Blood is a complex fluid with properties that are not yet fully known. Blood properties have been further characterized in terms of storage life (de Castro, Taylor et al. 2016), dependence on hematocrit (Chao, Trybala et al. 2014, Kim, Ma et al. 2016), and extensional viscosity (Kolbasov, Comiskey et al. 2016). Blood substitutes with analog rheology have been formulated and characterized (Yousif, Holdsworth et al. 2011, Najjari, Hinke et al. 2016, Brindise, Busse et al. 2018), and tested in the context of forensic applications (Stotesbury, Illes et al. 2017). Fluid dynamic models of the atomization of blood have been formulated and compared to experiments with backward (Comiskey, Yarin et al. 2017) and forward (Comiskey, Yarin et al. 2018) gunshot spatters. Quantitative measurements have estimated the initial velocities and drop sizes resulting from gunshots (Comiskey, Yarin et al. 2017) and impact spatter events (Das, Faflak et al. 2019). Trajectory models accounting for the effect of drag and gravity on drops were produced and calibrated (Kabaliuk, Jermy et al. 2014, Laan, de Bruin et al. 2015). The spreading of a dripping drop has been characterized as a function of the impact conditions on various non-absorbing target materials (Kim, Ma et al. 2016). The differences in size distribution between spatter patterns from gunshot and those from blunt impacts have been described quantitatively (Siu, Pender et al. 2017). Automated classification methods were developed (Arthur, Hoogenboom et al. 2018, Liu, Attinger et al. 2020) to classify blood spatters patterns according to the generation mechanism. Uncertainties related to fluid dynamic conditions on the determination of the impact angle from stain inspection have also been quantified (Lockard 2015). It was found that the fall height of a dripping drop could be determined from the target surface properties and the presence and abundance of spines in the periphery of the stain, a deformation due to a fluid dynamic instability (Hulse-Smith, Mehdizadeh et al. 2005). Quantitative differences have been identified between spatter stains on fabrics and their transfer onto fabrics by contact (Cho, Springer et al. 2015). Quantitative measurements were made of the wicking, rotation, and deformation of stains caused by fabrics (Agrawal, Barnet et al. 2017). It was found that the backing material and mounting method of a fabric influence the shape of drip stains (Chang and Michielsen 2016). Datasets of blood spatter patterns (Attinger, Liu et al. 2018, Attinger, Liu et al. 2019) have been made available, in high resolution, to the scientific community for the purpose of testing methods and data. State of the art image processing methods (Arthur, Humburg et al. 2017) were described to quantitatively describe the multitude of stains (more than 40,000 in some gunshot spatter patterns).

The studies mentioned above represent significant progress in addressing some of the challenges identified by the NRC report (NRC 2009). It is, however, not straightforward to transfer this fundamental knowledge into usable tools for forensic analysts. Academic findings must be packaged into methods that can be taught to industry practitioners. For wider acceptance, new forensic analysis methods and tools must be robust, easy to use, and offer a significant improvement over the state of the art. If possible, these tools should also provide estimations of uncertainty and error, which are important to court testimony.

In this manuscript, we investigate experimentally and theoretically the following problem relevant to crime scene reconstruction: *Assuming a relative position between a specific stain on fabric and a blood source, is it possible that a given stain – with measurable size – has originated from the assumed blood source – or not*? This question is related to the more general problem of how far a blood drop can travel, albeit formulated from the viewpoint of the analyst, who does not consider drops but stains. The proposed study combines a wide range of experiments with fluid dynamics modeling. Then, the solution to the above question is presented in a single chart that is simple to use for the analyst. The elaboration of the chart however is based on consideration of the relevant fluid dynamics mechanisms, including in-flight deformation of drops.

“How far can a drop travel? How far from its source can a blood stain be found?” These questions have been studied and answered in multiple ways. The locations of stains farthest away (horizontally) from a blood source have been measured in gunshot studies, using various guns, ammunition, and blood sources, such as bovine heads (Grabmuller, Cachee et al. 2016), a human cadaver filled with blood (Rossi, Herold et al. 2018), foams or sponges soaked in blood (Stephens and Allen 1983, Siu, Pender et al. 2017), or cavities filled with blood (Comiskey, Yarin et al. 2018). Examples of maximum distances reported are 0.7 m (Comiskey, Yarin et al. 2016) for gunshot backspatter patterns and 4 m (Comiskey, Yarin et al. 2018) for forward spatter patterns. An anonymous literature review in the 2007 newsletter of the International Association of Bloodstain Pattern Analyst (IABPA) (Anonymous 2007) mentions 12 references for “distance that backspatter travels”. Depending on the study cited, the maximum distances given are between 0.3 m (1 ft) and 2 m (6.5 ft). It is important to mention that the studies cited (Forest, Gaensslen et al. 1983, Pex and Vaughan 1987, Karger, Nüsse et al. 1996, Karger, Nüsse et al. 1997, James, Kish et al. 2005, MacDonell 2005) were not exclusively focused on the issue of how far a single drop can travel. Some studies were focused on how far drops forming sub-mm stains would travel (Bevel and Gardner 2002), while other were focused on the presence of stains on the hands holding the gun (Karger, Nüsse et al. 1996). A presentation at the 2018 IABPA conference called “Slugger Slaying Caught on Tape” (Bockrath and Lugo 2017) described a beating in a Walmart department store recorded by surveillance cameras. The victim, immobilized on the floor, had their head struck by repeated assaults with a baseball bat. The farthest stain was found 33 ft (10.1 m) away from the region of origin of the spatter, which, to the best of our knowledge, is the farthest on record.

Regarding the above problem on how far a stain on fabric can be found from its source, (Attinger 2019) has recently proposed charts to evaluate how far a stain can be found from its source on a non-absorbing surface. This manuscript investigates a related problem, albeit for the case of an absorbing fabric target. Stains on fabrics are known to behave differently (Bevel and Gardner 2008) than stains on non-absorbing surfaces (Kim, Ma et al. 2016): wicking of the blood into the fabric, driven by capillary forces, increases and deforms the stain area. This deformation happens after spreading has occurred, and modifies the stain ellipticity $\varepsilon = W/L$, where W and L are width and length of an ellipse fitted to the stain, as well as the direction of the main axis of the stain (Agrawal, Barnet et al. 2017). While the relation between stain size, drop size, and impact conditions is well understood for non-absorbing target materials (Adam 2012), little is known about how stain size relates to drop size and impact conditions on absorbing substrates (Dicken, Knock et al. 2019). The present work investigates this problem with a large number of experiments and formulates it in a theoretical manner with clearly stated assumptions. Experimental results and theory are found to be consistent for a specific knitted fabric, and a process is described to extend the method to other fabrics. The manuscript starts with a presentation of the theoretical framework, followed by a thorough description of the theoretical and experimental methods, the results, and their discussion.

## 2. FUNDAMENTAL QUESTION AND FRAMEWORK OF THE STUDY

The question underlying the present practical study is "*How far can a blood drop with given initial diameter d and initial velocity $V_0$ travel from its source?*" This corresponds to a physical and deterministic problem proceeding forward in time from well-known initial conditions.

Questions addressed by forensic investigators are not that simple; they typically tackle reconstruction scenarios which are complex inverse problems. In a bloody crime or accident, drop velocities and sizes are generally unknown. The available evidence is one or several stains, patterns thereof, or even lack of stains on a given target surface. The investigator can measure the orientations, sizes, and shapes of the stains. The question asked by the investigator is thus not the deterministic question above ("*How far can a blood drop travel from its source?*"), but the slightly different problem shown in Fig. 1: "A piece of fabric is at a relative position from a blood source specified by a horizontal distance *r* and a signed vertical distance *z*. The blood source is at height *h* and the ceiling is at height *H* above the floor. The blood source generates drops with a broad and realistic range of diameters, initial velocities, and launch angles. *Is it possible that a specific stain on the fabric, with known size, has originated from a blood source at an assumed relative location, or not*?" In the above crime scene reconstruction question, we measured the stain size as its equivalent diameter $d_S$ , defined in Fig. 1. We use equivalent diameter because it is simpler to estimate than stain area for the analyst, and avoids confusions related to the association of "stain size" with either stain width or length. In the case of a round stain, the equivalent diameter is simply the diameter of the stain. This crime scene reconstruction question could be solved by performing backward trajectory reconstruction from impact conditions inferred from stain inspection, as done in (Laan, de Bruin et al. 2015, Attinger 2016) for non-absorbing substrates. However, there is currently no method to reconstruct impact conditions by inspection of stains on an absorbing substrate, because wicking deforms the stains and rotates their main axis as shown in (Agrawal, Barnet et al. 2017). Here, we focus on the case where stains are on fabrics, and we perform experiments and simulations to provide answers, leading to a chart useful to crime scene reconstruction.

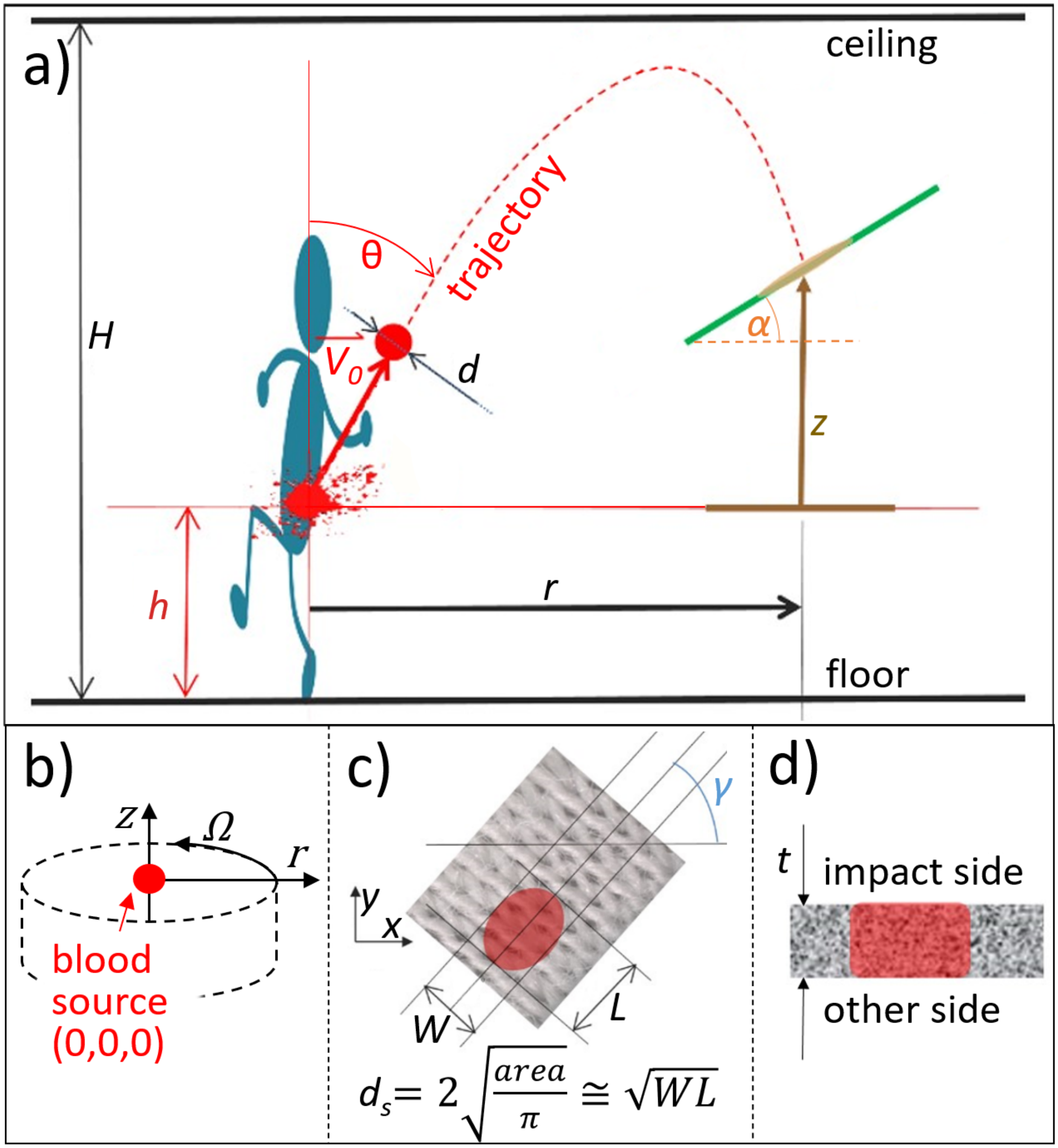


**Fig. 1** Representation of the problem "*How far can a blood drop travel from a blood source?*" The view orthogonal to the trajectory plane (a) illustrates the controlling variables of the forward problem: three heights (blood source $h$, ceiling $H$, and stain over blood source $z$), an orientation angle of the fabric swatch $\alpha$, one horizontal distance $r$ between stain and blood source, and three drop parameters (initial velocity $V_0$, launch angle $\theta$, and drop diameter $d$). The 3D projection of the cylindrical coordinates (b) explicitly shows distance $r$, azimuthal angle $\Omega$, and height $z$ relative to the blood source. The view from the top of the fabric (c) shows how the main direction of the stain corresponds to the direction of the impact $\gamma$ on non-absorbing surfaces, and how the area of the stain is used to estimate the equivalent stain diameter $d_S$. The view perpendicular to the fabric (d) shows that the stains considered have similar dimensions seen from both sides of a fabric with thickness $t$, an assumption necessary for the reconstruction method presented in this manuscript

# 3. METHODS

## 3.1 Experimental Methods

**Spatter experiments:** In this study, fluid dynamics experiments have been set up to investigate how far blood drops of various areas produced by an impact event can be found on fabric swatches. Blood used for this study is drawn from healthy swine at a USDA facility, and used within three days. Swine blood is considered an adequate and safer substitute for human blood in BPA experiments, with similar physical properties (Windberger, Bartholovitsch et al. 2003, Kolbasov, Comiskey et al. 2016, Attinger, Liu et al. 2020). The blood contains 1% of sodium heparin as an anticoagulant, and is stored in a refrigerator at 4°C in constant motion. Four experimental sessions are conducted, under the following range of conditions: Hematocrit 38 – 45 ± 1% (measured with an STI HemataSTAT-II® centrifuge); room temperature 16.5 – 22 ± 1°C; room relative humidity 43 – 72 ± 5%. Relevant fluid property values are in Sect. 3.2 below.

Experiments are performed in a shooting range or a spacious laboratory, both with minimal air currents. The blood source height ($h$) is set to 1 ± 0.01 m above the ground, and the ceiling height ($H$) of both rooms are measured as 2.6 ± 0.1 m. Fabric swatches are placed to capture stains at various horizontal distances ($r$), relative heights ($z$), and orientation angles ($\alpha$) with respect to the blood source, as listed in Table 1 and illustrated in Fig. 1a-b. In Cartesian coordinates, $r = \sqrt{x^2 + y^2}$, where the $x$-direction and $\Omega$ = 0° are the main spatter direction, aligned with the length of the room.

Each fabric swatch consists of a ~30x50 $cm^2$ rectangle cut out of an XL-sized white T-shirt, the specific fabric considered in this study, with properties listed in Table 2. The fabric was not ironed prior to the experiments. Fabric thickness $t$ is measured in accordance with the ASTM D1777-96 standard (ASTM 2015), under a reference pressure. We define the capacity Ø of a fabric to absorb liquids as the volume of liquid absorbed per volume of dry fabric. A simple way to estimate Ø consists in suspending a fabric sample with a known dry weight over a liquid pool with the bottom edge submerged, allowing liquid to wick into the fabric structure until equilibrium is reached. Then the wet sample is weighted again and the difference between dry and wet weight indicates the mass of liquid that has wicked into the fabric. Table 2 reports the capacity Ø measured with water, on a 6x3cm fabric sample, slightly folded along its main direction, held with clips like a tent with the two lower sides touching the liquid. Compared to blood, water is less viscous, has stronger surface tension and is devoid of particles, all properties that tend to maximize wicking and capillary filling. Note that Ø reported in Table 2 is larger than 1 because fabric thickness expands during the wicking process.

Swatches are mounted on butcher paper or cardstock backing (using glue around the perimeter of the fabric) with a tautness resembling that of clothes worn on the body.

Table 1: parameters used in the experiments

| Parameter, *symbol* [unit] | Number of possibilities | [list of comma-separated values] |
|---|---|---|
| **Ceiling height, *H* [m]** | 1 | [2.6] |
| **Blood source height, *h* [m]** | 1 | [1] |
| **Propagation distance, *r* [m]** | 10 | [1,2,3,4,4.5,5,5.5,6,7,8] |
| **Azimuthal angle, *Ω* [°]** | 1 | [0] |
| **Fabric height relative to blood source, *z* [m]** | 4 | [1,0,-0.9,-1] |
| **Fabric orientation, *α* [°]** | 3 | [0,45,90] |
| **Impact method** | 1 | [blunt impact] |

Table 2: Properties of the fabric used in this study

| | |
|---|---|
| **Designation** | Hanes ® white T-shirt |
| **Application and availability** | General purpose, available in retail stores |
| **Construction** | Single-jersey (stockinette) knit |
| **Composition (blends at yarn level)** | 60% cotton, 40% polyester |
| **Thickness, *t* (mm)** | 0.36 |
| **Capacity** Ø (null) | 1.47±0.07 |

The front surface (outside-facing) of the fabric is systematically oriented toward the blood source. The fabric swatches are oriented so that their wales, the visible diagonal lines made by the interlaced yarns, are vertical on vertical (α=90°) swatches or pointing towards the blood source on horizontal (α=0°) or angled (α=45°) swatches. In the fabric used, the wales correspond to the direction of fastest imbibition. Maintaining a common orientation is done to facilitate scanning and image post-processing.

Not directly relevant to this set of experiments but relevant to BPA in general is also the angle $\varphi$, the orientation of the fabric relative to a vertical axis. For this study, $\varphi$ is constant with the horizontal projection of the normal vector of the fabric plane pointing to the blood source, but other angles of $\varphi$ have been explored in (Faflak and Attinger 2019).

The position of stains is determined as the vector sum of a global vector pointing to a known location on the fabric swatch and a local vector on the fabric plane, resulting in global coordinate system $(r,\Omega,z)_{global}$ that describes the location of each stain, where the origin location $(0,0,0)_{global}$ is the blood source. Of the 120 possible combinations of parameters in Table 1, only 40 are tested due to considerations of redundancy.

Pictures of the experimental arrangement of fabric targets are in Fig. 2. Vertical fabric targets (α=90°) are mounted on structures built from silhouette stands made of wood lathe and rigid cardboard backing, reaching nearly to the ceiling. Horizontal fabric targets (α=0°) are laid either on the floor or on tables at the appropriate heights. Angled fabric targets (α=45°) are supported by rigid backing and set to the desired angle.

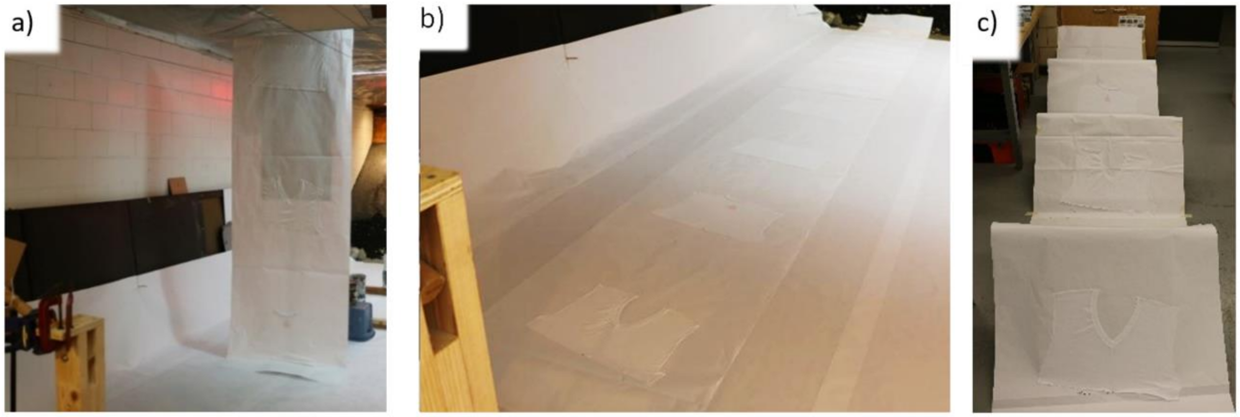


**Fig. 2** Positioning of fabric swatches vertically (a), horizontally (b), or at an angle (c)

Blood spatter patterns are generated using either a beating simulator called the Hockey Puck (HP) rig or a large slapping device inspired by the shape of a mousetrap (MT) device, both pictured in Fig. 3. These devices differ mainly by the kinematics of the impact, which significantly influences the spattering process (Attinger, Liu et al. 2018). On either device, a blood pool with a volume between 1 and 5 mL is placed on a level flat impact surface and impacted by a swinging hinged impactor. The impact velocity of the rotating rod arm end is varied between 5.2 and 7.8 ± 0.5 m/s on the HP rig, as measured in (Attinger, Liu et al. 2018), and 6.5 ± 0.3 m/s on the MT rig. For both impact spatter methods, impacts with target heights or distances at which fewer drops reach the target distance are repeated with various blood quantities or impact velocities until at least one stain with an equivalent diameter larger than 1.3 mm is observed on each fabric swatch of interest, or until blood ran out. Only stains with equivalent diameter larger than 1.3 mm are considered in the results of this study, to avoid confusing stains with fabric defects, and to be compatible with a volume conservation model described in section 3.2, which is used to relate the stain size to the drop size.

Experiments are performed with azimuthal angle $\Omega$ parallel to the main observed forward direction of the spatter. Subsequent experiments may explore the dependence of maximum flight distance on other angles.

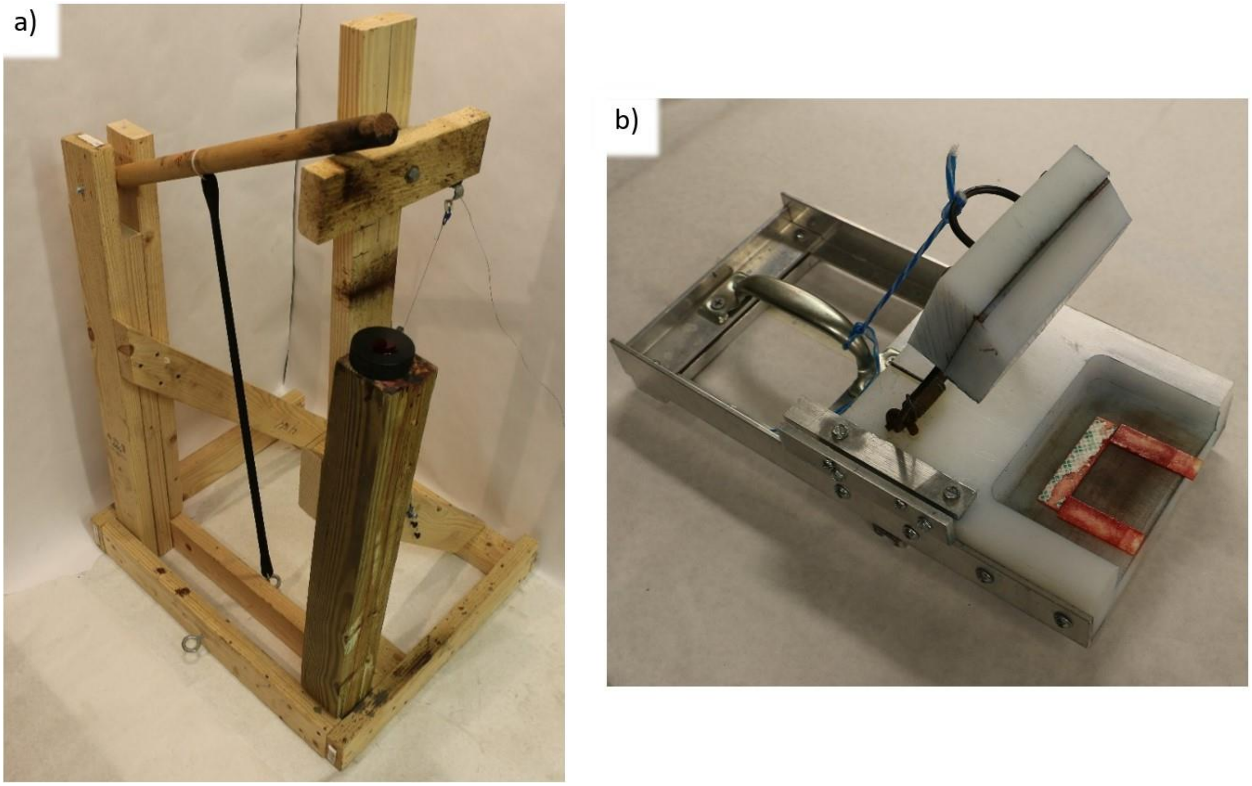

**Fig. 3** The devices used to generate blunt impact blood spatters: a) Hockey Puck beating simulator, where a cylindrical rod hits blood on a hockey puck (Attinger, Liu et al. 2018); b) mousetrap rig, where the blood is squeezed between two flat, parallel surfaces. The channel made from adhesive tape forces more blood to eject in the forward direction

**Measurement of stains:** Once the drop hits the ceiling, or the floor or fabric target, spreading and possibly wicking occur to create a stain. Measurements in (Agrawal, Barnet et al. 2017) show that the relation between drop and stain shape is of a different nature for absorbing materials such as fabrics versus non-absorbing surfaces such as cardstock or glass. On fabrics, stain ellipticity and direction is more difficult to measure and to interpret because wicking deforms the stains and significantly modifies their direction and ellipticity (Agrawal, Barnet et al. 2017). Information on stain ellipticity and direction is thus neglected in this study, where only information on stain size is used. While the angle of impact affects stain ellipticity and direction, it does not have a significant effect on the area of a stain on fabric, as shown in Fig. 4. Impact spatter data in Fig. 4 was obtained from gunshot backspatter patterns, with a 9mm Smith & Wesson handgun and round tip bullets (Attinger, Liu et al. 2019). Fabric was mounted on panels that prevented the muzzle gases to interact with the droplets. Stains were collected on white T-shirt fabric, oriented at different angles with respect to the general direction of the backspatter propagation. A first experiment spattered the fabrics set at oblique (60° and 45°) angles, and a second experiment spattered the fabric set at normal angle (90°). The average values and spread of the stain areas indicate that fabric orientation has little influence on the equivalent stain diameter. Each fabric swatch is scanned with an Epson Expression 11000XL flatbed scanner at 600 dpi, and the resulting images are saved in the .JPG file format. The images are then analyzed with a MATLAB code which outputs each stain's location and size.

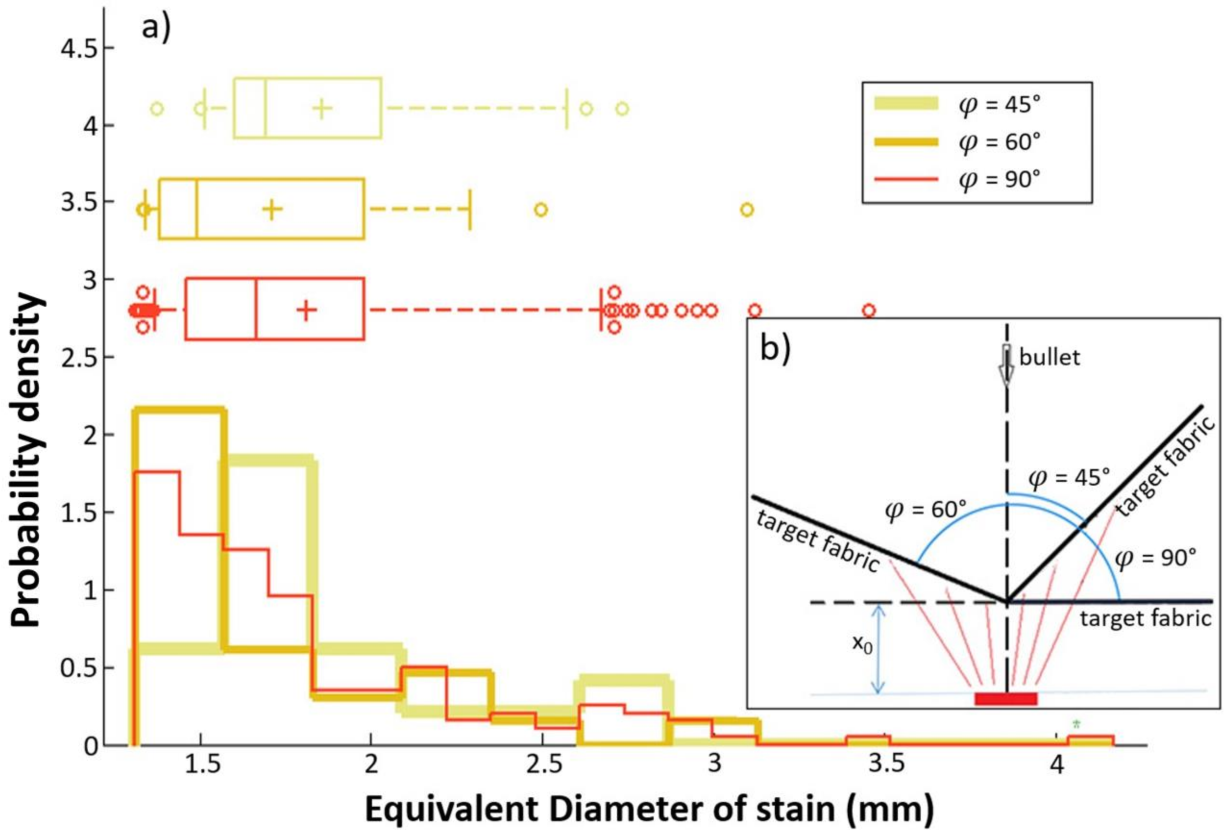


**Fig. 4** a) Set of histograms comparing the stain equivalent diameters on white T-shirt fabric from normal (90°) and oblique (60° and 45°) impact angles $\varphi$ from (Faflak and Attinger 2019), plotted with routines in (Lansey). The vertical axis shows probability density of stains to be of equivalent diameter on horizontal axis. Histograms are topped with boxplots representing data statistics: vertical line for median, '+' for mean, box around 25% and 75% quartiles, whiskers showing 9% and 91% of the distribution, and circles representing outliers. Inset b) is a schematic of fabric target setup used to produce histogram data, where the distance between blood source and fabric $x_0$ = 90 cm. Only stains with equivalent diameters ≥ 1.3 mm are reported.

A series of measurements on the relation between stain size and drop size have also been conducted, to characterize the numerical model developed in this study. The experiments and model are described together in the Sect. 3.2.

## 3.2 Theory and Numerical Methods

**Trajectories:** To interpret the experiments, we design and perform time-forward simulations of the droplet trajectories considering a representative range of initial conditions. A wide range of initial velocities, launch angles, and drop diameters is simulated, detailed in Table 3. The bounds of these values correspond to known or estimated limits of experiments with blood (Das, Faflak et al. 2019). It is assumed that the initial velocities, launch angles, and drop diameters are discretizing all the possible launching conditions with sufficient resolution.

Table 3: List of the discrete parameters used in the 39,585 trajectory simulations

| **Parameter, *symbol*, [unit]** | **Number of possibilities** | **[list of values separated by space]** |
|---|---|---|
| **Ceiling height above floor, *H*, [m]** | 1 | [2.6] |
| **Blood source height above floor, *h*, [m]** | 1 | [1] |
| **Launch angle, $\theta$, [°]** | 39 | [0 5 10 15 20 25 27.5 30 32.5 35 37.5 40 42.5 45 47.5 50 52.5 55 57.5 60 62.5 65 67.5 70 75 80 85 90 95 100 110 120 130 140 150 160 170 175 180] |
| **Drop diameter, *d*, [mm]** | 29 | [0.033 0.066 0.1 0.2 0.3 0.4 0.5 0.6 0.7 0.8 0.9 1 1.3. 1.6 2 2.3 2.6 3 3.3 3.6 4 4.5 5 5.5 6 7 8 9 10] |
| **Initial velocity, $V_0$, [m/s]** | 35 | [0.01 0.015 0.02 0.03 0.04 0.05 0.075 0.1 0.25 0.5 0.75 1 2 3 4 5 7.5 10 12.5 15 17.5 20 22.5 25 27.5 30 35 40 45 50 60 70 80 90 100] |

Much engineering literature exists describing the trajectories of flying drops, in studies of inkjet printing, fuel injection (Hsiang and Faeth 1995), or raindrops (Vargas 2013). A challenge in performing simulations such as those for this study is the expense of computational time and resources. Each trajectory is calculated by numerical integration of Newton's second law for a drop moving through the air, proceeding forward in time until the drop either contacts the ceiling or floor, or breaks up in flight due to drag force. The trajectories and drag force are simulated with the method described in (Attinger 2019), with the main equations provided in the supplementary documentation. The drag force model considers the deformation of drops in flight and the corresponding increase of drag. For some combinations of initial conditions in Table 3, the drag force overcomes the surface tension and the drop breaks up in flight. These cases have been removed from the dataset. Technically this represents a situation where the Weber ($We = \rho v^2 d/\sigma$) number reaches values larger than the critical value for break-up in flight, which is set to 13, consistent with experimental studies in (Hsiang and Faeth 1995). In fluid dynamics, *We* is a dimensionless parameter which characterizes the relation of inertial to surface forces as a function of the liquid's density, velocity through a medium, characteristic dimension, and surface tension. A blood drop flying through the air experiences its highest *We* at the moment of its highest velocity, which in this context (where velocity due to gravitational acceleration is insignificant) is the moment immediately after drop generation. Thus, a drop exceeding the critical *We* will have broken up soon after leaving the source location, yielding multiple drops with smaller diameters, the trajectories of which are included in the dataset. In-flight evaporation and aerodynamic interactions between drops are considered negligible. The following values are used for the physical properties of air and blood: density of blood $\rho = 1060$ kg/m$^3$; density of air $\rho_a = 1.229$ kg/m$^3$; surface tension between blood and air $\sigma$ = 59 mN/m; dynamic viscosity of blood $\mu$ =4.2x10$^{-3}$ Pa·s; dynamic viscosity of air $\mu_a =$ 1.98 x10$^{-5}$ Pa·s. The blood properties correspond to swine blood at temperature of 22°C and hematocrit of 45% (Kim, Ma et al. 2016). The simulated data set corresponds to about 40,000 trajectories, each corresponding to a different combination of the variables in Table 3.

**Estimation of stain size from computed drop impact conditions:** The spreading of a drop, and the relation between drop size and stain size is fundamentally different on absorbing materials such as fabrics vs. non-absorbing materials. On non-absorbing surfaces, spreading is mainly driven by inertial forces, while on fabrics, there is a concurrent or subsequent wicking that increases the area of the stain

(Agrawal, Barnet et al. 2017). On a non-absorbing surface, the spread factor ($\beta = d_s/d_{drop}$) has been shown to follow a power law of the product $Re^2Oh$, and is otherwise independent of the drop size (Scheller and Bousfield 1995). Above, the Reynolds number ($Re = \rho vd/\mu$) relates inertial and viscous forces, and the Ohnesorge number ($Oh = \sqrt{We}/Re$) relates viscous, inertial, and surface tension forces. Experiments with dripping drops on fabric reported in Fig. 5 show that the spread factor is mostly independent of $Re^2Oh$, and is rather a function of the drop volume, which we express with the following first order model. On fabrics, a relation between drop size and stain size can be established based on wicking and conservation of mass. Consider that all the volume of the drop is absorbed in the thickness of the fabric. Indeed, spatter stains in our experiments typically exhibit a similar stain area on the front and back of the fabric, without any bulge on the front or the back of the fabric. This indicates that the volume of the blood in the drop $V_d$ has been fully absorbed within the thickness of the fabric. The capacity Ø and thickness $t$ measured in Table 2 can determine the relation between drop size and stain size, by the following mass conservation argument.

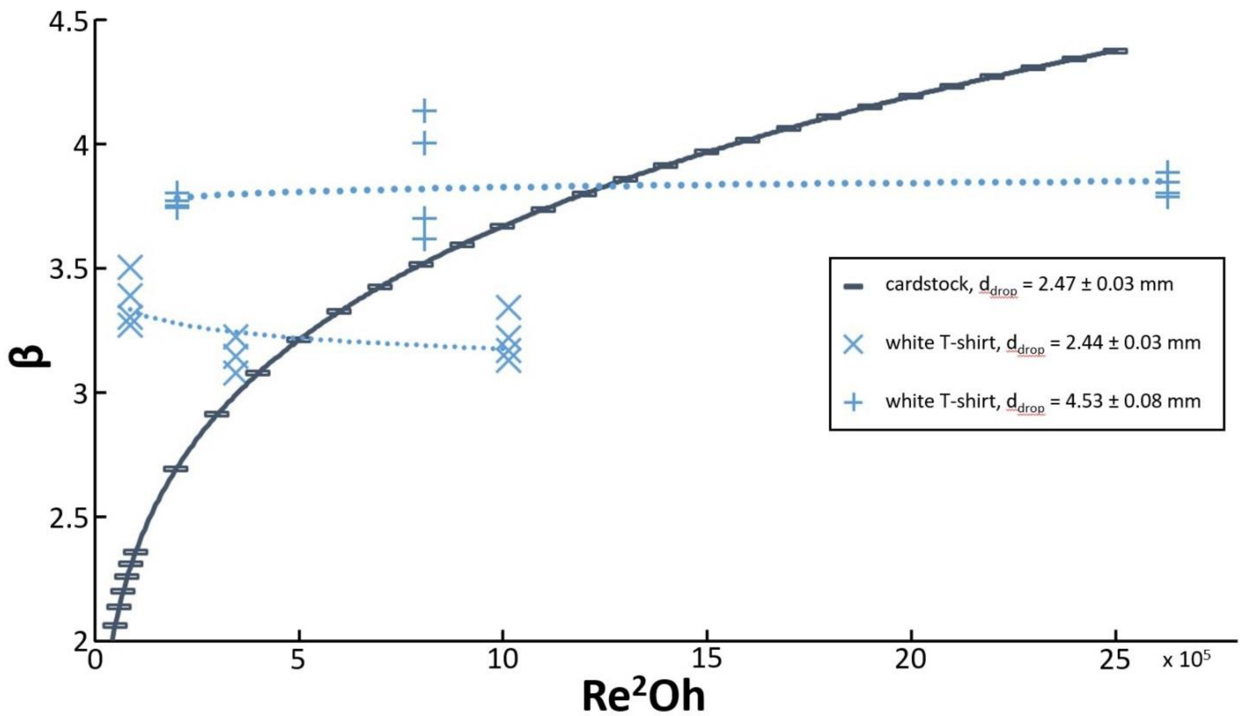


**Fig. 5** Spread Factor $\beta = d_s/d$ , ratio of stain diameter over drop diameter is plotted vs. the product of the Ohnesorge number and the square of the Reynolds number ($Re^2Oh$), a dimensionless measure of impact conditions, for blood drops on non-porous cardstock (solid line) and porous white T-shirt fabric (dotted lines)

Using mass conservation, we can write that the volume of blood in the drop equals the volume of blood fully absorbed as a stain in the fabric; $V_d = V_s$. Expressing both terms with respect to the variables defined above, we have

$$\frac{\pi d^3}{6} = \frac{\pi d_S^2}{4}(t\phi)_i, \tag{1}$$

and after simplification,

$$d_S^2 = C_i d^3, with\ C_i = \frac{2}{3(t\phi)_i} \tag{2}$$

The equivalent diameter of the stain $d_S$ is thus function of the size *d* of the impacting drop, and of a coefficient $C_i$, which according to the above derivation depends on the fabric of interest. The above equation allows the expression of trajectory simulation results either in terms of initial drop size or final stain size. While the former parameter is needed for the simulations, the latter is the one of interest for the forensic examiner. Each fabric has its own values of *t* and Ø, which we write as $(t\emptyset)_i$. The subscript *i* serves as a placeholder for the fabric of interest. $C_i$ can either be estimated based on the measured thickness and porosity of the fabric of interest, or estimated experimentally by measuring drop diameters and their resulting stain diameters in a controlled way. We have performed multiple experiments to determine the practical range of $C_i$ for the fabric of interest, by experimentally dripping blood drops of various sizes onto the fabric and relating drop volumes to the resulting stain sizes. We also have established a lower bound for $C_i$ by weighting the fully wet fabric.

Simulations using the trajectory and stain formation model presented above are conducted using the scientific computing language MATLAB version 2013b. Results (trajectories, impact conditions, stain sizes and locations) and corresponding input parameters (drop sizes and initial velocities) are saved into a structured data file. Numerical searching and sorting of the data set is then performed and compared with experimental measurements of stain positions and sizes obtained from impact patterns.

# 4. RESULTS

## 4.1 Experimental Results

Table 4 lists all fabric swatches investigated experimentally. Swatches were deployed up to 8 m away from the blood source, and no stains were recorded beyond 6 m. All the stained swatches were scanned into digital images, and a total of 2124 stains with equivalent diameters larger than 1.3 mm was automatically measured and counted. The absolute farthest stain was observed on the protective butcher paper floor covering at *r* = 5.74 m, *z* = -1 m, with an equivalent diameter of about 6 mm; the farthest stain on fabric landed at *r* = 5.65 m, *z* = -0.9 m with an equivalent diameter of about 4.8 mm.

Table 4: List, positions and spattering methods of the fabric swatches investigated. Grayed-out rows indicate fabrics that did not exhibit stains. Fabrics in other rows exhibited stains. The “Impact method” and “# of Impacts” are indicated. HP = Hockey Puck impact rig, MT = Mousetrap impact device. Merged cells indicate trials performed concurrently. Refer to Fig. 2 for images of fabric target positioning. In all cases, the height of the blood source above the floor *h* = 1 m and the ceiling height relative to the floor *H* = 2.6 m. The back of every fabric was labelled with α, *r* and *z* at the time of experiment. ID numbers are for reference.

<table>
<tr><th>Fabric ID</th><th>α [°]</th><th>r [m]</th><th>z [m]</th><th>Impact method</th><th># of Impacts</th></tr>
<tr><td>1</td><td>90</td><td>1</td><td>1</td><td rowspan="3">HP</td><td rowspan="3">3</td></tr>
<tr><td>2</td><td>90</td><td>1</td><td>0</td></tr>
<tr><td>3</td><td>90</td><td>1</td><td>-1</td></tr>
<tr><td>4</td><td>90</td><td>2</td><td>1</td><td rowspan="3">HP</td><td rowspan="3">3</td></tr>
<tr><td>5</td><td>90</td><td>2</td><td>0</td></tr>
<tr><td>6</td><td>90</td><td>2</td><td>-1</td></tr>
<tr><td>7</td><td>90</td><td>3</td><td>1</td><td rowspan="3">HP</td><td rowspan="3">6</td></tr>
<tr><td>8</td><td>90</td><td>3</td><td>0</td></tr>
<tr><td>9</td><td>90</td><td>3</td><td>-1</td></tr>
<tr><td>10</td><td>90</td><td>4</td><td>1</td><td rowspan="3">HP</td><td rowspan="3">7</td></tr>
<tr><td>11</td><td>90</td><td>4</td><td>0</td></tr>
<tr><td>12</td><td>90</td><td>4</td><td>-1</td></tr>
<tr><td>13</td><td>0</td><td>4.5</td><td>-0.9</td><td rowspan="4">MT</td><td rowspan="4">5</td></tr>
<tr><td>14</td><td>0</td><td>5</td><td>-0.9</td></tr>
<tr><td>15</td><td>0</td><td>5.5</td><td>-0.9</td></tr>
<tr><td>16</td><td>0</td><td>6</td><td>-0.9</td></tr>
<tr><td>17</td><td>0</td><td>4.5</td><td>0</td><td rowspan="4">MT</td><td rowspan="4">2</td></tr>
<tr><td>18</td><td>0</td><td>5</td><td>0</td></tr>
<tr><td>19</td><td>0</td><td>5.5</td><td>0</td></tr>
<tr><td>20</td><td>0</td><td>6</td><td>0</td></tr>
</table>

<table>
<tr><th>Fabric ID (cont.)</th><th>α [°]</th><th>r [m]</th><th>z [m]</th><th>Impact method</th><th># of Impacts</th></tr>
<tr><td>21</td><td>0</td><td>1</td><td>0</td><td rowspan="8">HP</td><td rowspan="8">15</td></tr>
<tr><td>22</td><td>0</td><td>2</td><td>0</td></tr>
<tr><td>23</td><td>0</td><td>3</td><td>0</td></tr>
<tr><td>24</td><td>0</td><td>4</td><td>0</td></tr>
<tr><td>25</td><td>0</td><td>5</td><td>0</td></tr>
<tr><td>26</td><td>0</td><td>6</td><td>0</td></tr>
<tr><td>27</td><td>0</td><td>7</td><td>0</td></tr>
<tr><td>28</td><td>0</td><td>8</td><td>0</td></tr>
<tr><td>29</td><td>0</td><td>1</td><td>-1</td><td rowspan="8">HP</td><td rowspan="8">16</td></tr>
<tr><td>30</td><td>0</td><td>2</td><td>-1</td></tr>
<tr><td>31</td><td>0</td><td>3</td><td>-1</td></tr>
<tr><td>32</td><td>0</td><td>4</td><td>-1</td></tr>
<tr><td>33</td><td>0</td><td>5</td><td>-1</td></tr>
<tr><td>34</td><td>0</td><td>6</td><td>-1</td></tr>
<tr><td>35</td><td>0</td><td>7</td><td>-1</td></tr>
<tr><td>36</td><td>0</td><td>8</td><td>-1</td></tr>
<tr><td>37</td><td>45</td><td>3</td><td>-1</td><td rowspan="4">MT</td><td rowspan="4">7</td></tr>
<tr><td>38</td><td>45</td><td>4</td><td>-1</td></tr>
<tr><td>39</td><td>45</td><td>5</td><td>-1</td></tr>
<tr><td>40</td><td>45</td><td>6</td><td>-1</td></tr>
</table>

For the sake of estimating drop size from stain size, we assume that each stain has the same size on the front and back of the fabric. To test the validity of this assumption, backside sections of three randomly selected fabric swatches were scanned in addition to the frontside (which was scanned for every swatch). Ratios of the areas of sample individual stains on the front vs. the back area were measured for a range of stain sizes, and reported in Fig. 6. The measurements show that for the specific fabric used in this study, an equivalent stain diameter of at least 1.3 mm is required to have stains with similar size on the frontside vs the backside of the fabric.

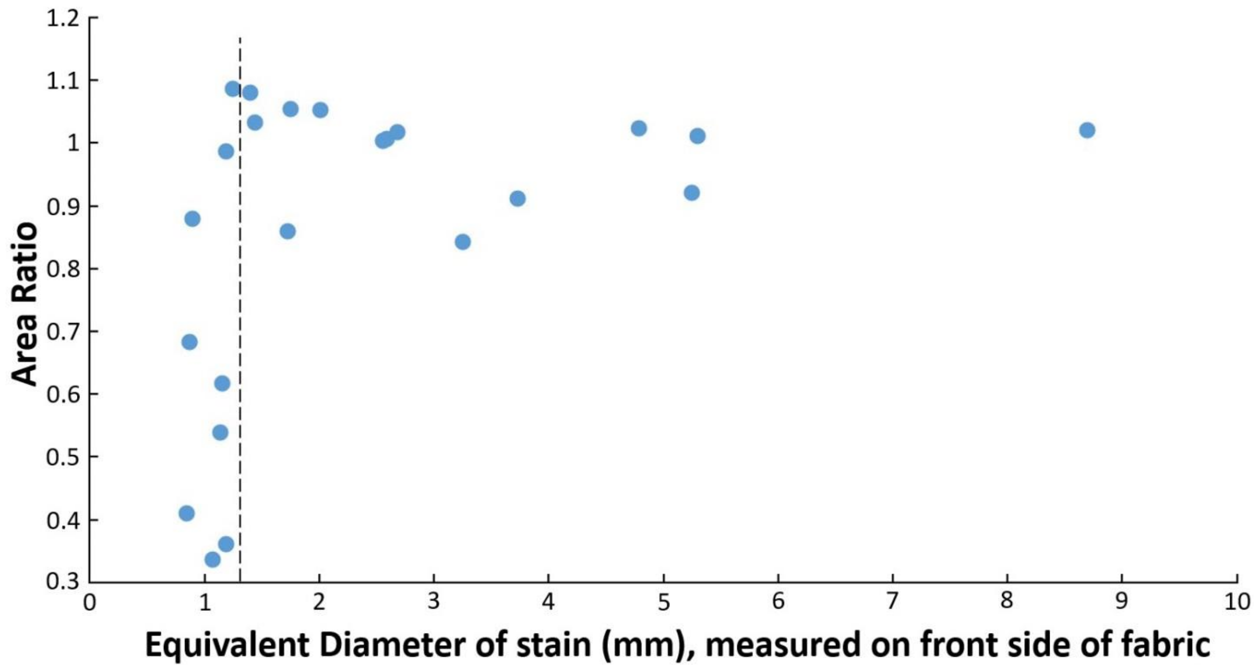


**Fig. 6** Ratios of the area of individual sample stains on the back vs. the front of white T-shirt fabric swatches, as a function of the equivalent diameter measured on the front side of the fabric. The dashed line denotes an equivalent diameter of 1.3 mm. Stains smaller than 1.3mm typically have larger stains on the back of the fabric than the front.

We also varied several experimental parameters to see how they influence the value of $C_i$. While there is currently no complete understanding of how drops of a complex fluid impact, spread and wick in a multiscale fabric (Wang, Gallardo et al. 2021), we investigated experimental combinations of the following variables susceptible to influence the values of $C_i$ with dripping drops: the size of the drop, the relative humidity (%RH) of the environment, the hematocrit (%H) of the blood, the mounting method (suspended taut or resting on a backing substrate), and the wear state of the fabric (expressed as w, the number of machine washes). Table 5 lists the experiments performed, where each combination was repeated *n*=3 to 16 times. Averaging the measurements with dripping drops over the 29 combinations of parameters investigated we obtain $C_i = 3.58$ mm$^{-1}$. For every combination of parameters and within one standard deviation, Table 5 shows that values of $C_i$ are in the interval $C_i =$ [2.33, 5.60 mm$^{-1}$].

Values of $C_i$ can also be determined from the measured thickness and capacity of the fabric in Table 2 These values obtained by weighting the water-soaked fabric are in the interval $C_i =$ [1.20, 1.32 mm$^{-1}$], and are smaller than the values obtained by dripping drops of blood. Likely, the blood wicks preferentially along some features of the fabric and leaves behind air voids in an amount that depends on, e.g., impact conditions and blood cell content. To illustrate the influence of the value of $C_i$ on the results, three values of $C_i$ will be used to compare the maximum distances predicted theoretically with the measured locations of the stain in the spatter experiments: the maximum value found from blood dripping experiments ($C_i = 5.60$ mm$^{-1}$), the minimum value found from blood dripping experiments ($C_i =$ 2.33 mm$^{-1}$), and the minimum value found from water absorption experiments ($C_i = 1.20$ mm$^{-1}$).

Table 5: List of experiments performed with dripping blood drops to determine the range of coefficient $C_i$ for white T-shirt fabric. From left to right, the columns indicate the drop diameter, the relative humidity, the hematocrit, the mounting method, the number of wash cycles, the number *n* of drops measured, and the orifice used to generate the dripping drops.

| $d_{drop}$, [mm] | %RH | %H | Mounting | Wash Cycles | n | orifice | $C_i$, [mm$^{-1}$] | St.Dev., [mm-1] | min $C_i$, [mm$^{-1}$] | max $C_i$, [mm$^{-1}$] |
|---|---|---|---|---|---|---|---|---|---|---|
| 4.75 | 18 | 36 | backed | 6 | 8 | luer | 2.45 | 0.12 | 2.33 | 2.57 |
| 4.75 | 18 | 36 | backed | 6 | 7 | luer | 2.47 | 0.08 | 2.39 | 2.55 |
| 2.43 | 18 | 36 | backed | 6 | 12 | 27 ga needle | 2.63 | 0.16 | 2.47 | 2.79 |
| 2.43 | 18 | 36 | backed | 6 | 12 | 27 ga needle | 2.65 | 0.14 | 2.51 | 2.79 |
| 2.45 | 50 | 36 | backed | 6 | 12 | 27 ga needle | 2.71 | 0.19 | 2.52 | 2.9 |
| 4.78 | 50 | 36 | backed | 6 | 6 | luer | 2.76 | 0.23 | 2.53 | 2.99 |
| 4.74 | 50 | 36 | backed | 6 | 6 | luer | 2.77 | 0.13 | 2.64 | 2.9 |
| 2.43 | 18 | 36 | backed | 6 | 15 | 27 ga needle | 2.77 | 0.11 | 2.66 | 2.88 |
| 2.45 | 50 | 36 | suspended | 6 | 14 | 27 ga needle | 2.88 | 0.15 | 2.73 | 3.03 |
| 2.23 | 50 | 36 | backed | 6 | 14 | 30 ga needle | 2.91 | 0.14 | 2.77 | 3.05 |
| 2.45 | 50 | 36 | backed | 6 | 14 | 27 ga needle | 2.97 | 0.13 | 2.84 | 3.1 |
| 2.23 | 50 | 36 | backed | 6 | 12 | 30 ga needle | 3.06 | 0.29 | 2.77 | 3.35 |
| 4.6 | 50 | 40 | suspended | 6 | 4 | luer | 3.19 | 0.07 | 3.12 | 3.26 |
| 2.23 | 50 | 36 | suspended | 6 | 14 | 30 ga needle | 3.23 | 0.18 | 3.05 | 3.41 |
| 4.36 | 50 | 40 | suspended | 6 | 4 | luer | 3.26 | 0.05 | 3.21 | 3.31 |
| 4.74 | 50 | 36 | suspended | 6 | 7 | luer | 3.29 | 0.14 | 3.15 | 3.43 |
| 4.74 | 50 | 36 | suspended | 6 | 7 | luer | 3.38 | 0.19 | 3.19 | 3.57 |
| 4.36 | 50 | 40 | suspended | 6 | 4 | luer | 3.44 | 0.44 | 3 | 3.88 |
| 2.45 | 50 | 36 | suspended | 6 | 14 | 27 ga needle | 3.86 | 0.34 | 3.52 | 4.2 |
| 2.47 | 50 | 40 | suspended | 6 | 3 | 27 ga needle | 4.02 | 0.19 | 3.83 | 4.21 |
| 4.68 | 95 | 36 | backed | 6 | 10 | luer | 4.2 | 0.13 | 4.07 | 4.33 |
| 2.44 | 50 | 40 | suspended | 6 | 4 | 27 ga needle | 4.24 | 0.24 | 4 | 4.48 |
| 2.43 | 95 | 36 | backed | 6 | 10 | 27 ga needle | 4.44 | 0.21 | 4.23 | 4.65 |
| 2.47 | 50 | 40 | suspended | 6 | 4 | 27 ga needle | 4.6 | 0.29 | 4.31 | 4.89 |
| 4.68 | 95 | 36 | suspended | 6 | 8 | luer | 4.76 | 0.18 | 4.58 | 4.94 |
| 2.5 | 50 | 42 | suspended | 0 | 5 | 27 ga needle | 5.12 | 0.19 | 4.93 | 5.31 |
| 2.43 | 95 | 36 | suspended | 6 | 12 | 27 ga needle | 5.19 | 0.41 | 4.78 | 5.6 |
| 2.5 | 50 | 42 | suspended | 0 | 5 | 27 ga needle | 5.23 | 0.18 | 5.05 | 5.41 |
| 2.5 | 50 | 42 | suspended | 0 | 5 | 27 ga needle | 5.24 | 0.15 | 5.09 | 5.39 |
| **Averages** | | | | | | | **3.58** | **0.19** | **2.33** | **5.60** |

The 3-dimensional positions and sizes of the stains obtained in the experiments are shown in Fig. 7. Each collected stain is represented at its location relative to the blood source. Colors correspond to the five ranges of stain equivalent diameter indicated in the legend. Only stains with equivalent diameters greater than 1.3 mm are shown. The green markers, representing stains smaller than 2 mm, are in the immediate vicinity of the blood source, because the smaller drops are most affected by drag and do not travel as far as larger drops launched under the same initial conditions.

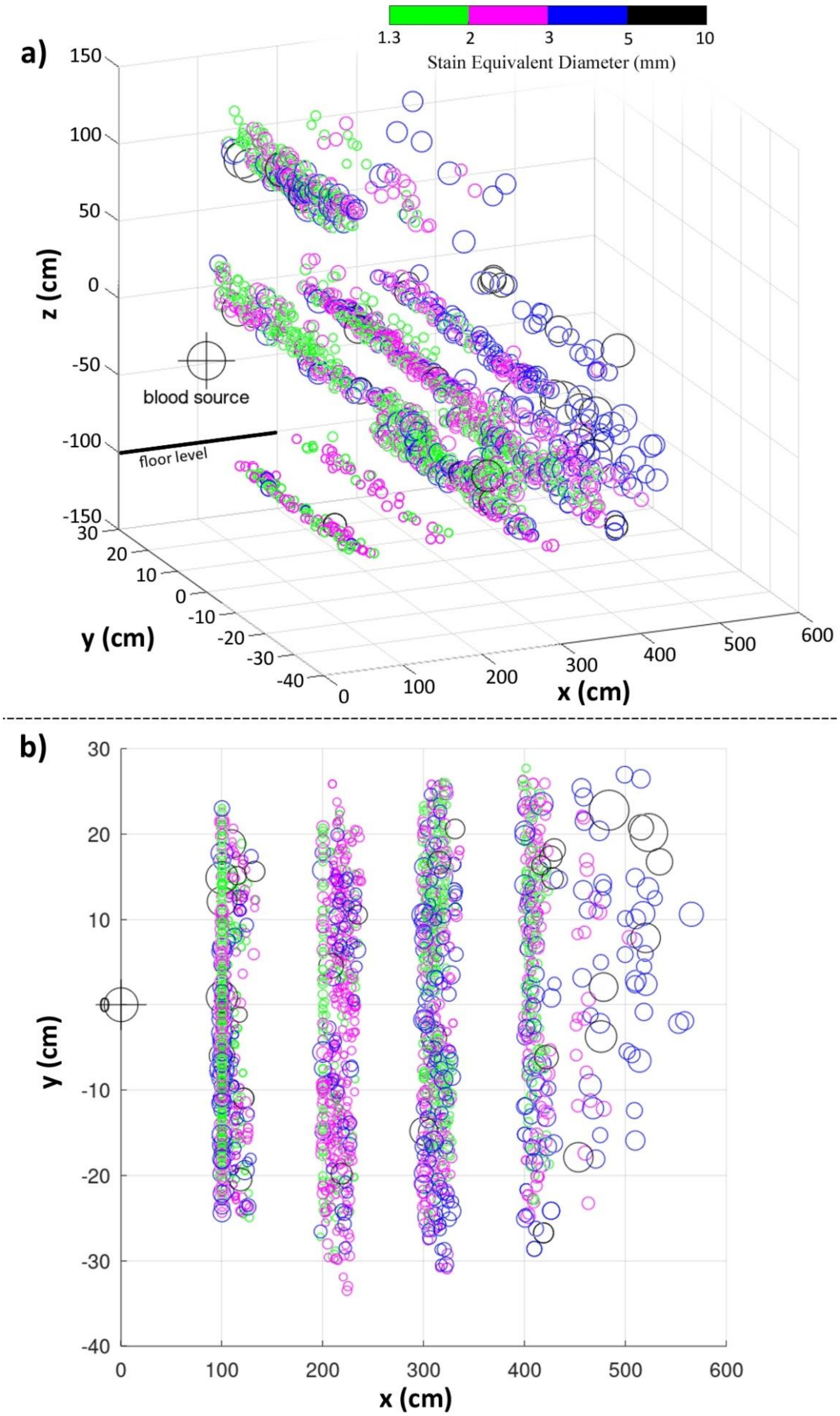
a)
1.3
2
3
5
10
Stain Equivalent Diameter (mm)
150
100
50
0
-50
-100
-150
z (cm)
blood source
floor level
30
20
10
0
-10
-20
-30
-40
y (cm)
0
100
200
300
400
500
600
x (cm)
b)
30
20
10
0
-10
-20
-30
-40
y (cm)
0
100
200
300
400
500
600
x (cm)

**Fig. 7** 3D plot, a) and top view plot, b) of all 2124 stain locations with sizes ≥ 1.3 mm generated in this study in $(x,y,z)_{global}$ space, where the blood source is located at (0,0,0). Axis *z* is oriented upwards. Marker areas are proportional to stain areas, and colors on the top bar represent ranges of equivalent diameter values

## 4.2 Numerical Results, with Comparison to Experiments

Numerical simulations of trajectories and stain formation are performed where the variables such as the height of blood source, drop diameter, and drop velocity assume any combination of values listed in Table 3. Fig. 8 describes the maximum distance between a stain on the floor and a blood source placed 1 m above the floor, in a room with the same ceiling height of 2.6 m as the one used in our experiments. The results are provided as a function of the initial drop diameter and velocity. A chart like Fig. 8 summarizes the many forward simulations performed in this study and allows the visualization of various aspects of the physics at hand. Unfortunately, it is of no practical use because drop diameters and initial velocities are unknown to the bloodstain pattern analyst. However, it informs on several aspects of the fluid dynamics at hand. First, Fig. 8 shows that the drops that can travel the farthest, in excess of 6 m, are those of average size ($d \in [2\ mm - 4\ mm]$ and average initial velocity ($V_0 \cong 12\ m/s$). The white region corresponds to cases where drag overcomes surface tension and the drop breaks up in flight, a situation described in Sect. 3.2 above. On the left side of the chart, smaller drops do not travel great distances – less than 1 m for drops smaller than 500 µm – because they encounter disproportionally strong drag with respect to their initial inertia. On the right side of the chart, larger drops can only be launched with velocities below 10 m/s to avoid break-up in flight. This explains why drops with intermediate sizes travel the farthest.

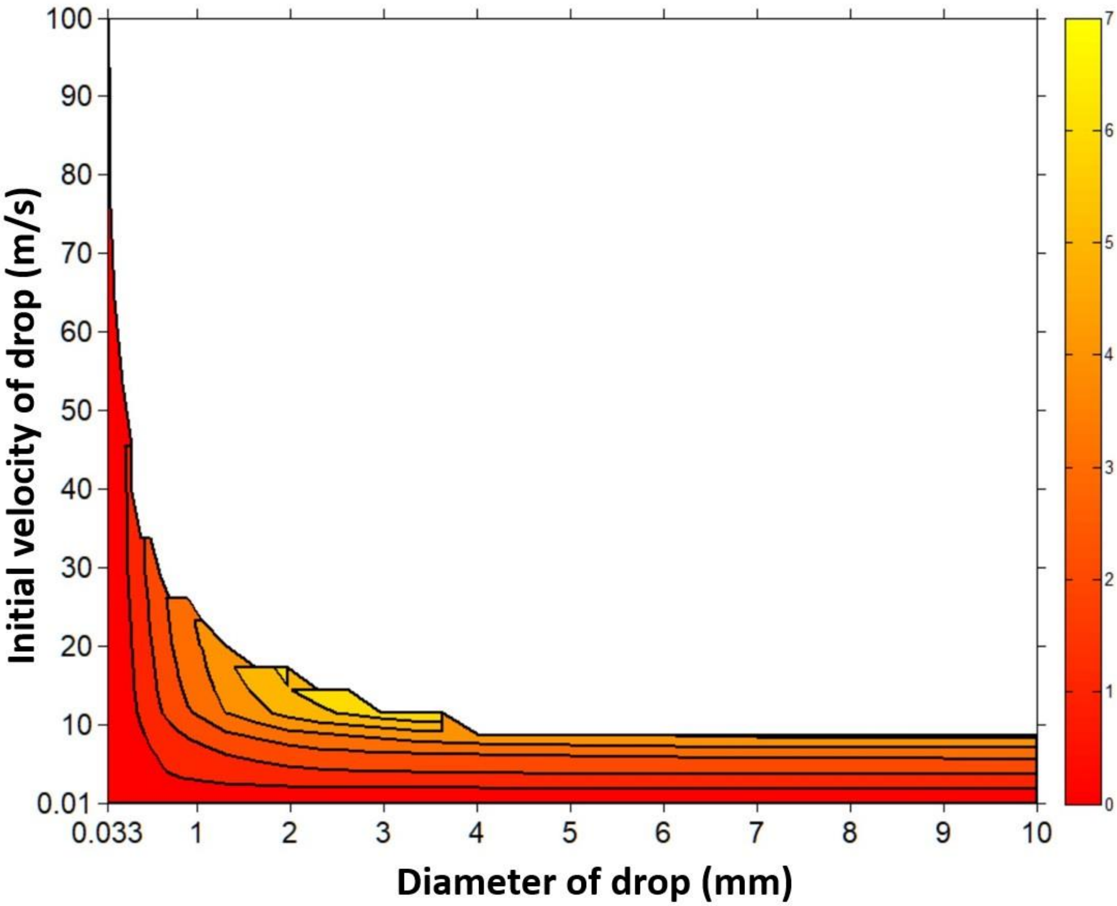


**Fig. 8** Maximum horizontal distance reached by a blood drop for the case where blood source is 1 m above the ground and ceiling is at 2.6 m. Horizontal distance in meters indicated by the color bar on the right between a stain and a blood source, as a function of the initial velocity of the drop and the diameter of the drop. Regions without color correspond to the drop breaking up in flight. Data generated assuming that variables can take any combination of values listed in Table 3.

While initial drop sizes cannot be determined in a crime scene, a parameter available to the bloodstain pattern analyst is the size of the stain, measured as its equivalent diameter, shown in Fig. 1b. Thus, the remainder of the results and discussion will deal with stain sizes rather than drop sizes, which allows comparison with experiments.

In Fig. 9, the blood source height ($h$) is set to 1 m above the floor and the ceiling height ($H$) is set to 2.6 m ($\cong$ 10 ft) which corresponds to the experimental configuration. The color curves in Fig. 9 show, based on numerical simulations of trajectories, the maximum heights $z$ and horizontal distances $r$ from the blood source, where stains with a range of equivalent diameter can be found. Height $z$ is a signed distance, meaning that a negative value of $z$ corresponds to the fabric being lower than the blood source, and a positive value, to the fabric being higher than the blood source. The stain is located at a horizontal distance $r$ of the blood source, on a fabric with arbitrary orientation. Curves in Fig. 9 correspond to three values of $C_i$ estimated above, respectively 1.20 mm$^{-1}$, 2.33 mm$^{-1}$ and 5.60 mm$^{-1}$. Predicted distances are moderately sensitive to the value of $C_i$ . Because $C_i = \frac{d_S^2}{d^3}$, smaller values of $C_i$ in Fig. 9 correspond to larger predicted distances for stains of a given size $d_S$, since the trajectory simulations are performed with set drop sizes $d$. The theoretical curves are generated assuming that the initial velocity, drop size, and the launch angle can take any combination of values listed in Table 3.

Superposed on the theoretical results are the experimental results for the 2124 measured stains. All stains are plotted in the (*r,z*) plane, with the location markers randomly shifted up to 5 cm in any direction to facilitate visualization. The clusters of stains are supplemented with pie charts illustrating the distribution of stain sizes within the five ranges of stain sizes. Each cluster occupies a volume of maximally 30x50x30 $cm^3$, and corresponds to the stains on one or multiple swatches of fabric. The experimental results in Fig. 9 are found in excellent agreement with the numerical results, in the sense that all measured stains are found within the theoretically predicted maximum distance and relative height, which are the solid curves with minimum value of $C_i$. Indeed, all the 2124 stains lie within the theoretical curves predicted with the smallest values $C_i = 1.20$ $mm^{-1}$. Theoretical results predicted with $C_i = 2.33$ $mm^{-1}$ are in agreement with the immense majority of the stains, except a small number of stains found on the floor (*z*=-1m) with measured sizes smaller than 3mm (magenta markers) and smaller than 2mm (green markers). Theoretical results predicted with $C_i = 5.60$ $mm^{-1}$ underestimate the experimental location of a large quantity of stains with measured sizes smaller than 5mm by up to one meter (the blue and cyan markers on the floor). Results of this comparison command to use the minimum value of $C_i = 1.20$ $mm^{-1}$ for estimating the maximum distance that a stain can be found from its source. Besides being the only among the three tested values that provides theoretical distances in agreement with all the stain locations measured in this work, this value of $C_i$ is obtained from simple measurements of fabric thickness, area, and dry vs. wet weight with water, contrary to the other two values of $C_i$ which require multiple dripping experiments with blood.

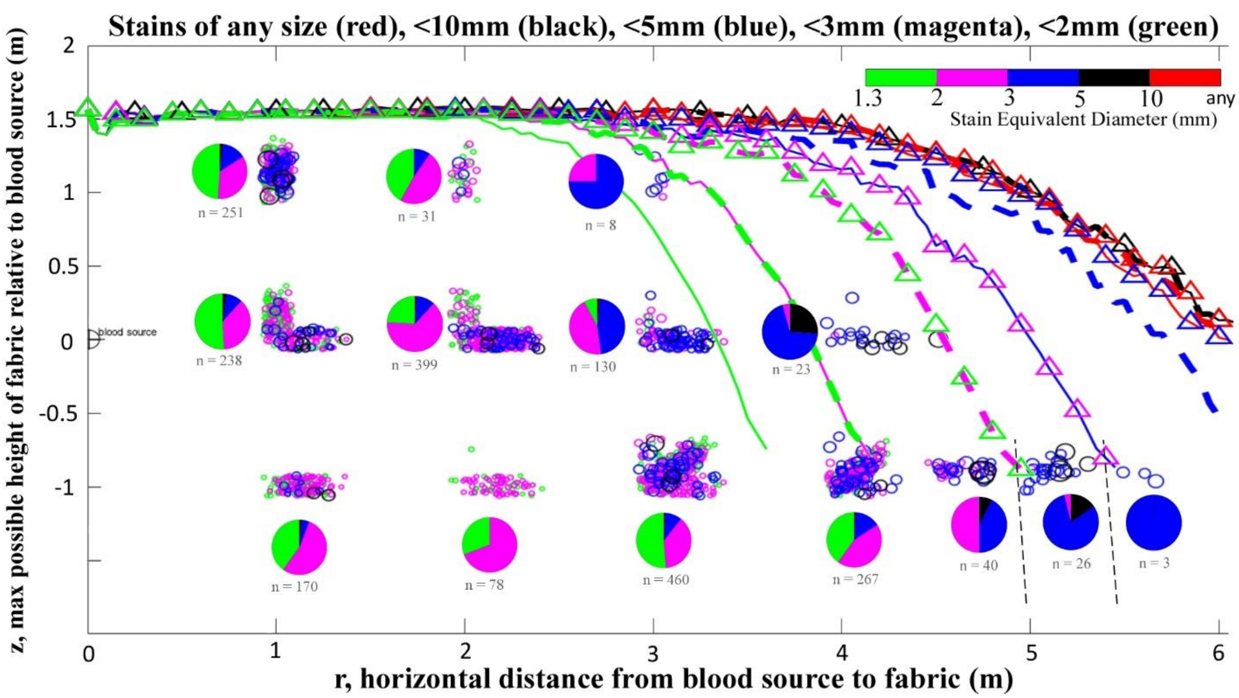


**Fig. 9** Plot in the (*r,z*) plane of the vertical and horizontal distances between stains on fabric and the blood source. Color curves are maximum distances obtained from numerical simulations. Colors in the plot refer to ranges of equivalent diameters of the stains as per the top scale bar. Circular markers describe the experimental positions of every measured stain. Individual marker areas are proportional to individual stain areas. Marker locations are randomly jittered up to 5 cm in any direction to aid visualization. The pie charts show the distribution of stain sizes per cluster; with number of stains *n* in each cluster, and the black dashed lines serve to distinguish nearby clusters. Each triplet of curves of a given color represent the maximum theoretical distance *r* for the following values of coefficient $C_i$ : 5.60 $mm^{-1}$ (solid line), 2.33 $mm^{-1}$ (dashed) and 1.20 $mm^{-1}$ (triangular markers).

## 4.3 Discussion and use for criminal investigations

The agreement between theoretical and experimental determination of the maximum distances between stains and blood source found in Fig. 9 can inspire a novel approach to crime scene reconstruction. Because the results of the simulations are provided as an organized and searchable data structure, it is possible to screen the numerical results for specific situations relevant to crime scene investigation. For instance, let us assume that the position of the blood source in a given room is known, from either testimony or investigative assumptions. The relative position between that blood source and fabric can be expressed with two values, $r_i$ and $z_i$, where $i$ is the index of the fabric, such as in the relative position of fabric “D” in the inset of Fig. 10. The dataset of simulations can thus be searched to determine if the assumed configuration is possible or not. The chart in Fig. 10 directly answers that question, for a blood source one meter above the floor.

The solid colored curves in Fig. 10 are to the maximum theoretical distances estimated from the trajectory simulations, for measured value of $C_i = 1.20\ mm^{-1}$, which corresponds to the largest possible travel distances based on the simulation set. These curves can be used to answer the question “*What is the farthest possible distance this drop could have traveled to form this stain?*”. The inset in Fig. 10 illustrates the way to determine if a spatter stain on a fabric could have originated from a blood source, given an assumed relative position between stain and blood source. The red volume is determined by the envelope of the curves of maximum distance. Thus, only a fabric within the red volume (“C” or “D”) could be stained by a spatter stain originating from the assumed source. Fabrics “A” and “B” are outside of the red volume and could not be stained by spatter stains originating from the pictured blood source.

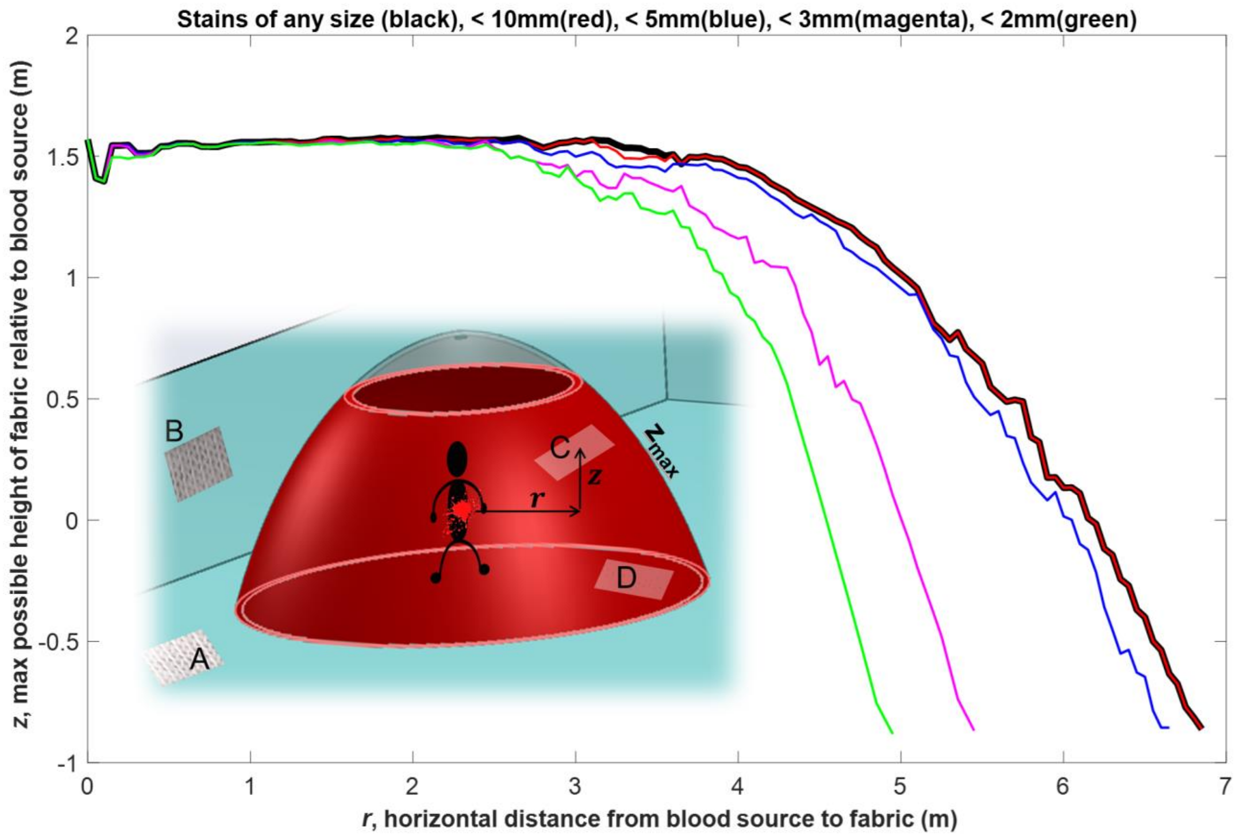


**Fig. 10** Chart to determine if a blood stain on fabric can originate from a blood source, for an assumed relative position of stain and source. Distance *r* in meters between a stain on fabric and its blood source is a function of the drop size and the height difference between the fabric and the blood source. Note that the colored lines in this figure correspond to the lines with triangular markers in Fig. 9. Inset illustrates how each colored distance curve distinguish a volume near the blood source (where fabrics can possibly be stained) from an outer region where fabric could not have been stained by drops issued from the source.

As an example, if T-shirt section of the inset of Fig. 10 is lying on a surface one meter high (*z* = 0) and has a stain measuring 4 mm in equivalent diameter, the blue curve shows that the corresponding blood source could have been as far horizontally as ~5.8 m.

These curves answer a question that currently cannot be answered in crime scene reconstruction – *"Could this stain on fabric have come from that source?"*. Note that the method in Fig. 10 does not rely on the ellipticity of stains. While the additional information would refine the reconstruction, fabrics modify the ellipticity and directionality of stains, as quantified by (Agrawal, Barnet et al. 2017), and it is not clear at present how the impact angles and direction of trajectory can be reliably deduced from a stain on fabric. The method described in this study however allows the analyst to determine if a stain on fabric can originate from a blood source assuming that their relative position in space is known. The chart provided in Fig. 10 is specific to the white T-shirt fabric used in this study. It can be considered to be similar to a "ballistic table" in that outcomes are given over discreet intervals (the stain sizes) by varying a few parameters (*r* and *z*) and holding all other parameters constant.

It is important to state the assumptions underlying the calculations while interpreting the numerical results.

1. Drops are of a fluid with properties same as those of swine blood at 22°C (Attinger, Moore et al. 2013).
2. Evaporation is neglected.
3. Effects of mild indoor air currents on the drop trajectories is considered negligible. See (Kabaliuk, Jermy et al. 2014) for estimates of those effects. Similarly, it is assumed that in case of gunshot spatters, muzzle gases do not modify the drop trajectories.
4. Each drop travels independently from any other, thus neglecting the ‘bird formation flight’ effect in (Comiskey, Yarin et al. 2017). Consideration of this drag reduction effect might increase the maximum distance between drop and source, especially for situations where the launch angle is within a narrow range, such as jets (Comiskey and Yarin 2018) in arterial gushing.
5. If a drop splashes upon impact into a main drop and smaller cast-off drops, the volume of the main drop is not affected significantly, and none of the cast-off drops produce stains larger than the minimum equivalent threshold diameter of 1.3 mm.
6. The sizes of stains on fabrics depend mainly on drop size and the kind of fabric. Dependence on other variables such as impact angle and velocity is not significant.
7. The stain size is same at the front and back of the fabric. Practically, this criterion corresponds to a ratio of their areas within 90 and 110%.

Regarding assumption (5), the experiments in this study did not produce any identifiable cast-off features on fabric swatches located at $r \geq 3m$ from the blood source. We define cast-off features as those stains which are a) proximate within a distance of three times the parent stain’s largest dimension, and b) at least an order of magnitude smaller than the parent stain. On porous media such as fabrics, cast-off stains are less likely to occur than on non-porous media (Okawa, Shiraishi et al. 2006) given similar impact conditions, and those that might occur would likely be smaller than the threshold stain diameter for analysis of 1.3 mm. Closer swatches proved to be too dense with stains of a wide range of sizes to ascertain such a conclusion; even so, results of this study pertain to stains at relatively great distances from their blood source. While it is also theoretically possible that two drops land on top of each other and create a stain unusually larger, this possibility is unlikely because the stained area in our experiments drops below 5% of the total area as soon as the horizontal distance from source to fabric reaches one meter.

# 5. CONCLUSION

Experiments have been performed that study impact spatter stains on a knitted fabric. A total number of 2124 stains are identified and measured. The maximum distance between the stains and the blood source was measured and found to correlate with the stain size. Results are presented as a function of stain size, a feature which is easily measured on the crime scene. A simple model of stain formation on fabric was proposed. Numerical simulations of the related trajectories were also developed and performed, for combinations of a wide range of the following variables: drop diameter, drop initial velocity and launch angle, height of blood source, and height of ceiling. The experimental results were found to be in excellent agreement with the numerical results. The study proposes a new investigative tool for crime scene reconstruction: a chart that determines if a given stain – with a measured equivalent diameter on a specific fabric – can originate from a given blood source, assuming a specific relative position between fabric and source.

It is the opinion of the authors that the packaging of complex physics into easy-to-use charts can offer novel tools for forensic investigators. Packaging a multiplicity of fluid dynamic simulations into a tool that is simple to use and that does not require any knowledge of fluid dynamics is analog to a pregnancy test. Disposable pregnancy tests package complex chemistry, biology, and fluid dynamics in a reliable and easy-to-use manner, and in this case, yields a definitive yes or no answer to the question *“Could this stain have come from that source?”*. As such, the “pregnancy test” approach presented in this work is worth refining and making available as a tool for the BPA practitioner, along with the classical approach of teaching fluid dynamics to bloodstain pattern analysts. Interpretation of the method on a crime scene is simple and does not require extensive knowledge of fluid dynamics.

It must be reiterated that the method is valid as long as the minimum of $C_i$ of the fabric in question is known. The results presented in this work are thus only valid for the white T-shirt fabric used. To use the method with other fabrics specific to a given crime scene, calibration measurements are required to obtain the specific minimum of $C_i$. Future work will explore the values of $C_i$ for other fabrics, and the possibility to produce charts such as Fig. 10 valid for a wide range of fabrics typically found on crime scenes.

# 6. REFERENCES


Adam, C. D. (2012). "Fundamental studies of bloodstain formation and characteristics." Forensic Sci Int(219): 76-87.

Adam, C. D. (2013). "Experimental and theoretical studies of the spreading of bloodstains on painted surfaces." Forensic Sci Int **229**(1-3): 66-74.

Agrawal, P., L. Barnet and D. Attinger (2017). "Bloodstains on woven fabric: Simulations and experiments for quantifying the uncertainty on the impact and directional angles." Forensic Science International **278**: 240-252.

Anonymous (2007). "literature search for the distance that backspatter travels." IABPA News **23**(3, September 2017): 31-32.

Arthur, R. M., J. Hoogenboom, M. Baiker, M. C. Taylor and K. G. de Bruin (2018). "An automated approach to the classification of impact spatter and cast-off bloodstain patterns." Forensic Sci Int **289**: 310-319.

Arthur, R. M., P. J. Humburg, J. Hoogenboom, M. Baiker, M. C. Taylor and K. G. de Bruin (2017). "An image-processing methodology for extracting bloodstain pattern features." Forensic Science International **277**: 122-132.

ASTM (2015). ASTM D1777-96(2015) Standard Test Method for Thickness of Textile Materials. West Conshohocken, PA; ASTM International.

Attinger, D. (2016). Development of a Science Base and Open Source Software for Bloodstain Pattern Analysis, Final technical report, 2010-DN-BX-K403.

Attinger, D. (2019). "Charts based on millions of fluid dynamics simulations provide a simple tool to estimate how far from its source a specific blood stain can be found." Forensic Sci Int **298**: 97-105.

Attinger, D., Y. Liu, T. Bybee and K. De Brabanter (2018). "A data set of bloodstain patterns for teaching and research in bloodstain pattern analysis: Impact beating spatters." Data in Brief **18**: 648-654.

Attinger, D., Y. Liu and K. De Brabanter (2020). "Authors' Response." J Forensic Sci **65**(4): 1386-1387.

Attinger, D., Y. Liu, R. Faflak, Y. Rao, B. A. Struttman, K. De Brabanter, P. M. Comiskey and A. L. Yarin (2019). "A data set of bloodstain patterns for teaching and research in bloodstain pattern analysis: gunshot backspatters." Data in Brief **22**: 269-278.

Attinger, D., C. Moore, A. Donaldson, A. Jafari and H. A. Stone (2013). "Fluid dynamics topics in bloodstain pattern analysis: comparative review and research opportunities." Forensic Sci Int **231**(1-3): 375-396.

Bevel, T. and R. M. Gardner (2002). Bloodstain Pattern Analysis with an Introduction to Crime Scene Reconstruction, CRC Press, Boca Raton, FL, USA.

Bevel, T. and R. M. Gardner (2008). Bloodstain Pattern Analysis with an Introduction to Crime Scene Reconstruction, Third Edition, CRC Press, Boca Raton, FL, USA.

Bockrath, J. and R. Lugo (2017). Slugger Slaying Caught on Tape. 2017 Annual IABPA Training Conference (International Association of Bloodstain Pattern Analysts), Crown Plaza Redondo Beach and Marina.

Brindise, M. C., M. M. Busse and P. P. Vlachos (2018). "Density- and viscosity-matched Newtonian and non-Newtonian blood-analog solutions with PDMS refractive index." Experiments in Fluids **59**(11).

Buck, U. and B. Kneubuehl (2012). "Response to "3D bloodstain pattern analysis: Ballistic reconstruction of the trajectories of blood drops and determination of the centres of origin of the bloodstains" by Buck et al. [Forensic Sci. Int. 206 (2011) 22-28]." Forensic Sci Int.

Camana, F. (2013). "Determining the area of convergence in Bloodstain Pattern Analysis: A probabilistic approach." Forensic Science International **231**(1-3): 131-136.

Chang, J. Y. M. and S. Michielsen (2016). "Effect of fabric mounting method and backing material on bloodstain patterns of drip stains on textiles." International Journal of Legal Medicine **130**(3): 649-659.

Chao, T. C., A. Trybala, V. Starov and D. B. Das (2014). "Influence of haematocrit level on the kinetics of blood spreading on thin porous medium during dried blood spot sampling." Colloids and Surfaces A: Physicochemical and Engineering Aspects **451**: 38-47.

Cho, Y., F. Springer, F. A. Tulleners and W. D. Ristenpart (2015). "Quantitative bloodstain analysis: Differentiation of contact transfer patterns versus spatter patterns on fabric via microscopic inspection." Forensic Science International **249**: 233-240.

Comiskey, P. M. and A. L. Yarin (2018). "Friction coefficient of an intact free liquid jet moving in air." Experiments in Fluids **59**(4).

Comiskey, P. M. and A. L. Yarin (2019). "Self-similar turbulent vortex rings: interaction of propellant gases with blood backspatter and the transport of gunshot residue." Journal of Fluid Mechanics **876**: 859-880.

Comiskey, P. M., A. L. Yarin and D. Attinger (2017). "High-Speed Video Analysis of Forward and Backward Spattered Blood Droplets." Forensic Science International **276**: 134-141.

Comiskey, P. M., A. L. Yarin and D. Attinger (2017). "Hydrodynamics of back spatter by blunt bullet gunshot with a link to bloodstain pattern analysis." Physical Review Fluids **2**(7): 073906.

Comiskey, P. M., A. L. Yarin and D. Attinger (2018). "Theoretical and experimental investigation of forward spatter of blood from a gunshot." Physical Review Fluids **3**(6): 063901.

Comiskey, P. M., A. L. Yarin, S. Kim and D. Attinger (2016). "Prediction of blood back spatter from a gunshot in bloodstain pattern analysis." Physical Review Fluids **1**(4): 043201.

Das, R., R. Faflak, D. Attinger and J. B. Michael (2019). Blood atomization from blunt impact on a liquid film using high-speed digital in-line holography. ILASS-Americas 30th Annual Conference on Liquid Atomization and Spray Systems, Tempe, AZ**:** CD-ROM proceedings.

de Castro, T. C., M. C. Taylor, D. J. Carr, J. Athens and J. A. Kieser (2016). "Storage life of whole porcine blood used for bloodstain pattern analysis." Canadian Society of Forensic Science Journal **49**(1): 26-37.

Dicken, L., C. Knock, D. J. Carr and S. Beckett (2019). "The effect of fabric mass per unit area and blood impact velocity on bloodstain morphology." Forensic Sci Int **301**: 12-27.

Faflak, R. and D. Attinger (2019). Bloodstain Pattern Analysis on US Military Fabrics (a report of 233 pages), Cooperative Agreement Number W911NF-15-2-0111 with the U.S. Army Research Office and the Defense Forensic Science Center (DFSC) 233 pages.
Feng, C., S. Michielsen and D. Attinger (2018). "Impact of carpet construction on fluid penetration: The case of blood." Forensic Sci Int **284**: 184-193.
Forest, P. R. D., R. E. Gaensslen and H. C. Lee (1983). Forensic science: An introduction to criminalistics, McGraw-Hill, New York.
Grabmuller, M., P. Cachee, B. Madea and C. Courts (2016). "How far does it get?--The effect of shooting distance and type of firearm on the simultaneous analysis of DNA and RNA from backspatter recovered from inside and outside surfaces of firearms." Forensic Sci Int **258**: 11-18.
Hsiang, L. P. and G. M. Faeth (1995). "Drop deformation and breakup due to shock-wave and steady disturbances." International Journal of Multiphase Flow **21**(4): 545-560.
Hulse-Smith, L., N. Z. Mehdizadeh and S. Chandra (2005). "Deducing drop size and impact velocity from circular bloodstains." Journal of Forensic Sciences **50**(1): 54-63.
James, S. H., P. E. Kish and T. P. Sutton (2005). Principles of Bloodstain Pattern Analysis: Theory and Practice, CRC Press.
Kabaliuk, N., M. C. Jermy, E. Williams, T. L. Laber and M. C. Taylor (2014). "Experimental validation of a numerical model for predicting the trajectory of blood drops in typical crime scene conditions, including droplet deformation and breakup, with a study of the effect of indoor air currents and wind on typical spatter drop trajectories." Forensic Sci Int **245**: 107-120.
Karger, B., R. Nüsse, B. Brinkmann, G. Schroeder and S. Wüstenbecker (1996). "Backspatter from experimental close-range shots to the head: 1. Macrobackspatter." International journal of legal medicine **109**(2): 66-74.
Karger, B., R. Nüsse, H. D. Tröger and B. Brinkmann (1997). "Backspatter from experimental close-range shots to the head: 2. Microbackspatter and the morphology of bloodstains." Int J Legal Med **110**: 27-30.
Kim, S., Y. Ma, P. Agrawal and D. Attinger (2016). "How important is it to consider target properties and hematocrit in bloodstain pattern analysis?" Forensic Science International **266**: 178-184.
Kolbasov, A., P. Comiskey, R. P. Sahu, S. Sinha-Ray, A. L. Yarin, B. S. Sikarwar, S. Kim, T. Z. Jubery and D. Attinger (2016). "Blood Rheology in Shear and Uniaxial Elongation." Rheologica Acta **55**: 901-908.
Kröll, A. K., M. Kettner, P. Schmidt and F. Ramsthaler (2017). "A novel experimental approach for classifying blood trails in relation to three different speeds of movement." Rechtsmedizin **27**(6): 528-535.
Laan, N., K. G. de Bruin, D. Slenter, J. Wilhelm, M. Jermy and D. Bonn (2015). "Bloodstain Pattern Analysis: implementation of a fluid dynamic model for position determination of victims." Sci Rep **5**: 11461.
Lansey, J. C. "Plot and compare histograms; pretty by default, 2015."
Liu, Y., D. Attinger and K. De Brabanter (2020). "Automatic Classification of Bloodstain Patterns Caused by Gunshot and Blunt Impact at Various Distances." Journal of Forensic Sciences **65**(3): 729-743.
Lockard, M. (2015). THE FLUID DYNAMICS OF DROPLET IMPACTS ON INCLINED SURFACES WITH APPLICATION TO FORENSIC BLOOD-SPATTER ANALYSIS, MS Thesis, Georgia Tech.
MacDonell, H. L. (2005). Bloodstain Patterns, Laboratory of Forensic Sciences, Corning, NY USA.
Najjari, M. R., J. A. Hinke, K. V. Bulusu and M. W. Plesniak (2016). "On the rheology of refractive-index-matched, non-Newtonian blood-analog fluids for PIV experiments." Experiments in Fluids **57**(6).
NRC (2009). Strengthening Forensic Science in the United States: A Path Forward, Committee on Identifying the Needs of the Forensic Sciences Community, National Research Council (National Research Council. Washington, DC: The National Academies Press**:** 177-179.
Okawa, T., T. Shiraishi and T. Mori (2006). "Production of secondary drops during the single water drop impact onto a plane water surface." Experiments in Fluids **41**(6): 965-974.

Pex, J. O. and C. H. Vaughan (1987). "Observations of high velocity bloodspatter on adjacent objects." Journal of Forensic Sciences **32**(6): 1587-1594.

Rossi, C., L. D. Herold, T. Bevel, L. McCauley and S. Guadarrama (2018). "Cranial Backspatter Pattern Production Utilizing Human Cadavers." J Forensic Sci **63**(5): 1526-1532.

Scheller, B. L. and D. W. Bousfield (1995). "Newtonian drop impact with a solid surface." AICHE Journal **41**(6): 1357-1367.

Shiri, S., K. F. Martin and J. C. Bird (2018). "Surface coatings including fingerprint residues can significantly alter the size and shape of bloodstains." Forensic Sci Int **295**: 189-198.

Siu, S., J. Pender, F. Springer, F. Tulleners and W. Ristenpart (2017). "Quantitative Differentiation of Bloodstain Patterns Resulting from Gunshot and Blunt Force Impacts." J Forensic Sci: 1-14.

Stephens, B. G. and T. B. Allen (1983). "Back spatter of blood from gunshot wounds. Observations and experimental simulation." Journal of Forensic Sciences **28**(2): 437-439.

Stotesbury, T., M. Illes, P. Wilson and A. J. Vreugdenhil (2017). "The application of silicon sol-gel technology to forensic blood substitute development: Investigation of the spreading dynamics onto a paper surface." Forensic Science International **275**: 308-313.

Vargas, M. (2013). "Drag Coefficient of Water Droplets Approaching the Leading Edge of an Airfoil." 5th AIAA Atmospheric and Space Environments Conference: 1-23, DOI:10.2514/2516.2013-3054.

Wang, F., V. Gallardo, S. Michielsen and T. Fang (2021). "Fundamental study of porcine drip bloodstains on fabrics: Blood droplet impact and wicking dynamics." Forensic Science International **318**: 110614.

Windberger, U., A. Bartholovitsch, R. Plasenzotti, K. J. Korak and G. Heinze (2003). "Whole blood viscosity, plasma viscosity and erythrocyte aggregation in nine mammalian species: reference values and comparison of data." Experimental Physiology **88**(3): 431-440.

Yousif, M. Y., D. W. Holdsworth and T. L. Poepping (2011). "A blood-mimicking fluid for particle image velocimetry with silicone vascular models." Experiments in Fluids **50**(3): 769-774.